

# A Joint Precoding Framework for Wideband Reconfigurable Intelligent Surface-Aided Cell-Free Network

Zijian Zhang, *Student Member, IEEE*, Linglong Dai, *Senior Member, IEEE*

**Abstract**—Thanks to the strong ability against the inter-cell interference, cell-free network has been considered as a promising technique to improve the network capacity of future wireless systems. However, for further capacity enhancement, it requires to deploy more base stations (BSs) with high cost and power consumption. To address the issue, inspired by the recently proposed technique called reconfigurable intelligent surface (RIS), we propose the concept of RIS-aided cell-free network to improve the network capacity with low cost and power consumption. The key idea is to replace some of the required BSs by low-cost and energy-efficient RISs, and deploy more RISs in the cell-free network for capacity enhancement. Then, for the proposed RIS-aided cell-free network in the typical wideband scenario, we formulate the joint precoding design problem at the BSs and RISs to maximize the network capacity. Due to the non-convexity and high complexity of the formulated problem, we develop an alternating optimization algorithm to solve this challenging problem. In particular, we decouple this problem via Lagrangian dual transform and fractional programming, and solve the subproblems alternatively. Note that most of the considered scenarios in existing works are special cases of the general scenario in this paper, and the proposed joint precoding framework can also serve as a general solution to maximize the capacity in most of existing RIS-aided scenarios. Finally, simulation results verify that, compared with the conventional cell-free network, the network capacity of the proposed scheme can be improved significantly.

**Index Terms**—Cell-free network, reconfigurable intelligent surface (RIS), wideband, joint precoding.

## I. INTRODUCTION

Network technique is the most essential technique to increase the capacity of wireless communication systems [1]. Compared with 4G, the capacity of 5G wireless network is expected to be increased by about 1000 times [2]. In the currently deployed cellular networks, all users in a cell are mainly served by one base station (BS), thus the users close to the cell boundary usually suffer from the severe inter-cell interference, which is caused by the signals from adjacent cells.

Ultra-dense network (UDN) has been proposed as a promising technique for 5G to further enhance the network capacity

[3], [4]. The key idea of UDN is to increase the number of BSs and deploy small cells [5] in the *cell-centric* cellular network. However, as the increase of the cell density, the inter-cell interference grows larger and larger. The cooperation theory has determined that [6], the upper limit of the network capacity will be bounded by the inter-cell interference as long as the network-centric network is used. In other words, inter-cell interference becomes the bottleneck for the network capacity improvement of UDN. This problem is inherent to the cell-centric network paradigm, and cannot be efficiently solved [7].

To address the issue, a novel *user-centric* network paradigm called cell-free network has been recently proposed [7]. Unlike the classical cell-centric design principle, the cell-free network utilizes the user-centric transmission design, where all BSs in the network jointly serve all users cooperatively without cell boundaries. Due to the efficient cooperation among all distributed BSs [8], the inter-cell interference can be effectively alleviated, and thus the network capacity can be increased accordingly. This promising technique has been considered as a potential candidate for future communication system [9], and has attracted the increasing research interest such as resource allocation [10], precoding/beamforming [11], channel estimation [12] in recent years.

However, to improve the network capacity further, the deployment of more distributed synchronized BSs requires high cost and power consumption in the cell-free network. Fortunately, the emerging new technique called reconfigurable intelligent surface (RIS) is able to provide an energy-efficient alternative to enhance the network capacity. Equipped with a low-cost, energy-efficient and high-gain metasurface, RIS is becoming a promising smart radio technique for future 6G communications [13]. With a large number of low-cost passive elements, RIS is able to reflect the electromagnetic incident signals to any directions with extra high array gains by adjusting the phase shifts of its elements [14]. Since the wireless environment can be effectively manipulated with low cost and energy consumption [15], RIS can be used to improve the channel capacity [16], reduce the transmit power [17], enhance the transmission reliability [18], and enlarge the wireless coverage [19].

## A. Prior works

The existing research works about RIS include antenna design [20], channel estimation [21], joint precoding/beamforming [22], and etc. Particularly, the prototype of

All authors are with the Beijing National Research Center for Information Science and Technology (BNRist) as well as the Department of Electronic Engineering, Tsinghua University, Beijing 100084, China (e-mails: zhangzijian@mails.tsinghua.edu.cn, daill@tsinghua.edu.cn).

This work was supported by the National Science and Technology Major Project of China under Grant 2018ZX03001004-003 and the National Natural Science Foundation of China for Outstanding Young Scholars under Grant 61722109.

RIS-based wireless communication has been recently developed in [23] to demonstrate its function in real systems.

One key guarantee for RIS to improve the network capacity is the joint precoding. Different from the conventional precoding at the BS only, the joint precoding in RIS-based wireless systems refers to the joint design of the beamforming vector at the BS and the phase shifts of the RIS elements. Different RIS-based scenarios have been studied to maximize the capacity in the literature. Specifically, the authors in [24] considered a scenario where one BS and one RIS jointly serve a single user, which was an early attempt to realize the capacity enhancement by using low-cost and energy-efficient RIS. In [25], the authors considered a multi-user scenario and maximized the sum-rate of all users. To obtain the cooperation gain, the multi-BS scenario was considered in [19], while the multi-RIS case was investigated in [18], respectively. Besides, to satisfy the requirements of wideband system, the multi-carrier scenario has been discussed in [26].

Apart from the capacity maximization, the design goal for joint precoding can be different. Specifically, to reduce the power consumption, some researchers have proposed the methods to minimize the transmit power subject to the constraints of the user requirements [17], and the authors in [15] have developed a method to maximize the energy efficiency. Some researchers have considered the fairness among users, and some methods have been proposed to maximize the minimum signal-to-interference-plus-noise ratio (SINR) [22], [27]. In addition, minimizing the symbol error rate (SER) was considered in [28].

Moreover, RIS has been combined with different techniques in the literature. For instance, the RIS-aided millimeter-wave (mmWave) system was considered in [18] and [29], where the authors discussed the signal-to-noise ratio (SNR) maximization problem and the joint hybrid precoding design, respectively. In [26] and [30], the application of RIS in wideband orthogonal frequency division multiplexing (OFDM) systems was discussed to maximize the sum-rate. Moreover, in [19] and [27], the authors considered the cooperation of BSs and RIS in a multi-cell system. How to exploit RIS to enhance the performance of non-orthogonal multiple access (NOMA) systems was discussed in [31]. In addition, the secure transmission via RIS has been investigated in [32], and RIS was also considered to assist the communication using unmanned aerial vehicles (UAVs) [33].

### B. Our contributions

To address the challenge of cell-free network as mentioned above, in this paper we consider to exploit RISs to realize the improvement of network capacity with low cost and power consumption. Specifically, the contributions of this paper can be summarized as follows.

- We propose the concept of RIS-aided cell-free network to further improve the network capacity of the cell-free network with low cost and power consumption. The key idea is to replace some of the BSs in cell-free network by the energy-efficient RISs and deploy more RISs in the system for capacity enhancement. In the

proposed RIS-aided cell-free network, all BSs and RISs are simultaneously serving all users cooperatively. To the best of our knowledge, this is the first attempt to exploit RIS in cell-free network to improve the network capacity.

- For the proposed RIS-aided cell-free network in the typical wideband scenario, we formulate the joint precoding design problem at the BSs and RISs to maximize the weighted sum-rate (WSR) of all users to optimize the network capacity. Since the considered scenario is very general, i.e., multiple antennas, multiple BSs, multiple RISs, multiple users, and multiple carriers, most of the considered scenarios in existing works, such as single BS, single RIS, single user, and single carrier, or some of them are multiple, are all special cases of the considered scenario in this paper.
- Inspired by the methods introduced in [34] [35], we propose a joint precoding framework to solve the formulated WSR maximization problem. Specifically, the proposed framework is an alternating optimization algorithm, which can approximate the local optimal solution gradually. We first decouple the active precoding at the BSs and the passive precoding at the RISs via Lagrangian dual reformulation and fractional programming. Then, the decoupled subproblems are reformulated as the quadratically constrained quadratic program (QCQP) problems, respectively. By solving the subproblems alternatively, the WSR will converge to a local optimal solution. The simulation results show that RISs can improve the cell-free network capacity significantly. Note that the proposed joint precoding framework can also serve as a general solution to maximize the WSR in most of the existing RIS-aided scenarios in the literature.

### C. Organization and notation

*Organization:* The rest of the paper is organized as follows. The system model of the proposed RIS-aided cell-free network and corresponding WSR maximization problem formulation of joint precoding design are discussed in Section II. The joint precoding framework to solve the formulated problem is proposed in Section III. Numerical simulation results are provided in Section IV to validate the performance of the proposed joint precoding framework for the RIS-aided cell-free network. Finally, in Section V, conclusions are drawn and future works are discussed.

*Notations:*  $\mathbb{C}$ ,  $\mathbb{R}$ , and  $\mathbb{R}^+$  denote the set of complex, real, and positive real numbers, respectively;  $[\cdot]^{-1}$ ,  $[\cdot]^*$ ,  $[\cdot]^T$ , and  $[\cdot]^H$  denote the inverse, conjugate, transpose, and conjugate-transpose operations, respectively;  $\|\cdot\|$  denotes the Euclidean norm of its argument;  $\mathbb{E}\{\cdot\}$  is the expectation operator;  $\text{diag}(\cdot)$  denotes the diagonal operation;  $\Re\{\cdot\}$  denotes the real part of its argument;  $\otimes$  denotes the Kronecker product;  $\angle[\cdot]$  denotes the angle of its complex argument;  $\mathbf{I}_L$  is an  $L \times L$  identity matrix, and  $\mathbf{0}_L$  is an  $L \times L$  zero matrix; Finally,  $\mathbf{e}_l$  is an elementary vector with a one at the  $l$ -th position, and  $\mathbf{1}_L$  indicates an  $L$ -length vector with all elements are 1.

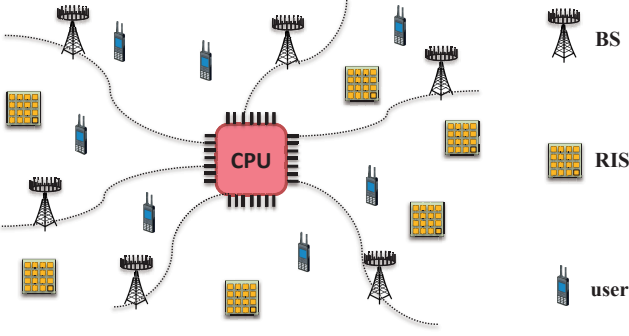


Fig. 1. The proposed concept of RIS-aided cell-free network.

## II. SYSTEM MODEL OF THE PROPOSED RIS-AIDED CELL-FREE NETWORK

To increase the network capacity with low cost and power consumption, in this paper we first propose the concept of RIS-aided cell-free network. Different from the traditional cell-free system, we replace some BSs by RISs and add more RISs in the network, where multiple BSs and multiple RISs are simultaneously employed to serve multiple users cooperatively. In this section, the architecture of the proposed RIS-aided cell-free network will be introduced at first. Then, we will discuss the transmitters, channels, and receivers, respectively. Finally, we will formulate the problem of capacity maximization problem in the RIS-aided cell-free network.

### A. System architecture

In this paper, we consider a wideband RIS-aided cell-free network as shown in Fig. 1, where multiple distributed BSs and RISs are deployed to cooperatively serve all users. A central processing unit (CPU) is deployed for control and planning, to which all BSs are connected by optical cables or wireless backhaul [36]. All RISs are controlled by the CPU or BSs by wire or wireless control. The considered network consists of  $B$  BSs,  $R$  RISs, and  $K$  multi-antenna users. The number of antennas at the  $b$ -th BS and that at the  $k$ -th user are  $M_b$  and  $U_k$ , respectively. The number of elements at the  $r$ -th RIS is  $N_r$ . For simplicity but without loss of generality, we assume  $M_b$ ,  $U_b$  and  $N_r$  are equal to  $M$ ,  $U$  and  $N$ , respectively. Finally, the multi-carrier transmission is considered and the number of available subcarriers is  $P$ . Let  $\mathcal{M} = \{1, \dots, M\}$ ,  $\mathcal{U} = \{1, \dots, U\}$ ,  $\mathcal{N} = \{1, \dots, N\}$ ,  $\mathcal{B} = \{1, \dots, B\}$ ,  $\mathcal{R} = \{1, \dots, R\}$ ,  $\mathcal{K} = \{1, \dots, K\}$  and  $\mathcal{P} = \{1, \dots, P\}$  denote the index sets of BS antennas, user antennas, RIS elements, BSs, RISs, users, and subcarriers, respectively.

### B. Transmitters

In the proposed RIS-aided cell-free network, all BSs are synchronized, which is necessary to serve all users by coherent joint transmission [8]. We follow the common assumption in the literature that all BSs transmit the same symbols [11], [37]–[39]. Let  $\mathbf{s}_p \triangleq [s_{p,1}, \dots, s_{p,K}]^T \in \mathbb{C}^K$ , where  $s_{p,k}$

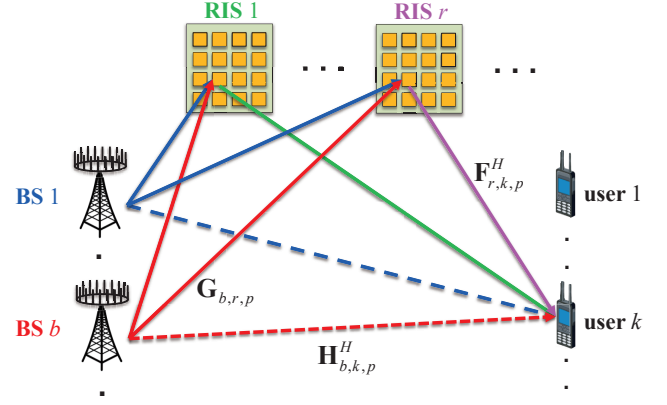


Fig. 2. The downlink channels in the wideband RIS-aided cell-free network.

denotes the transmitted symbol to the  $k$ -th user on the  $p$ -th subcarrier. We assume that the transmitted symbols have normalized power, i.e.,  $\mathbb{E}\{\mathbf{s}_p \mathbf{s}_p^H\} = \mathbf{I}_K, \forall p \in \mathcal{P}$ . In the downlink, the frequency-domain symbol  $s_{p,k}$  is firstly precoded by the precoding vector  $\mathbf{w}_{b,p,k} \in \mathbb{C}^M$  at the  $b$ -th BS, so the precoded symbol  $\mathbf{x}_{b,p}$  at the  $b$ -th BS on the  $p$ -th subcarrier can be written as

$$\mathbf{x}_{b,p} = \sum_{k=1}^K \mathbf{w}_{b,p,k} s_{p,k}. \quad (1)$$

Then, by inverse discrete Fourier transform (IDFT), the frequency-domain signal  $\{\mathbf{x}_{b,p}\}_{p=1}^P$  on all  $P$  subcarriers at the  $b$ -th BS is converted to the time domain. After adding the cyclic prefix (CP), the signal is up-converted to the radio frequency (RF) domain via  $M$  RF chains of the  $b$ -th BS.<sup>1</sup>

### C. Channels

Thanks to the directional reflection supported by  $R$  RISs, as shown in Fig. 2, the channel between each BS and each user in the proposed RIS-aided cell-free network consists of two parts: the BS-user link and  $R$  BS-RIS-user links, where each BS-RIS-user link can be further divided into a BS-RIS link and a RIS-user link. The signal reflection on the RISs can be modeled by multiplying the incident signal with a phase shift matrix and forwarding the phase shifted signal to the user [24]. Therefore, the equivalent channel  $\mathbf{h}_{b,k,p}^H$  from the  $b$ -th BS to the  $k$ -th user on the  $p$ -th subcarrier can be written as [41]

$$\mathbf{h}_{b,k,p}^H = \underbrace{\mathbf{H}_{b,k,p}^H}_{\text{BS-user link}} + \sum_{r=1}^R \underbrace{\mathbf{F}_{r,k,p}^H \mathbf{\Theta}_r^H \mathbf{G}_{b,r,p}}_{\text{BS-RIS-user links}}, \quad (2)$$

where  $\mathbf{H}_{b,k,p}^H \in \mathbb{C}^{U \times M}$ ,  $\mathbf{G}_{b,r,p} \in \mathbb{C}^{N \times M}$ , and  $\mathbf{F}_{r,k,p}^H \in \mathbb{C}^{U \times N}$  denote the frequency-domain channel on the subcarrier  $p$  from the BS  $b$  to the user  $k$ , from the BS  $b$  to the RIS  $r$ , and from the RIS  $r$  to the user  $k$ , respectively;  $\mathbf{\Theta}_r \in \mathbb{C}^{N \times N}$  denotes the phase shift matrix at the RIS  $r$ , which is written as

$$\mathbf{\Theta}_r \triangleq \text{diag}(\theta_{r,1}, \dots, \theta_{r,N}), \quad \forall r \in \mathcal{R}, \quad (3)$$

<sup>1</sup>In this paper, the fully-digital precoding is considered for the proposed RIS-aided cell-free network, since usually the number of BS antennas is not very large. The extension to the hybrid precoding [40] is left for future work.

where  $\theta_{r,n} \in \mathcal{F}$ . Note that  $\mathcal{F}$  is the feasible set of the reflection coefficient (RC) at RIS. Here we assume  $\mathcal{F}$  is the ideal RIS case, i.e., both the amplitude and the phase of  $\theta_{r,n}$  associated with the RIS element can be controlled independently and continuously, i.e.,

$$\mathcal{F} \triangleq \left\{ \theta_{r,n} \mid |\theta_{r,n}| \leq 1 \right\}, \quad \forall r \in \mathcal{R}, \quad \forall n \in \mathcal{N}. \quad (4)$$

Note that the more practical RIS reflection coefficients such as low-resolution discrete phase shifts will be discussed in Subsection III-E later.

#### D. Receivers

After passing through the equivalent channel  $\mathbf{h}_{b,k,p}^H$  as shown in (2), the signals will be received by the users. The time-domain signals received by the users are down-converted to the baseband at first. After the CP removal and the discrete Fourier transform (DFT), the frequency-domain symbols can be finally recovered. Let  $\mathbf{y}_{b,k,p} \in \mathbb{C}^U$  denote the baseband frequency-domain signal, which is received by the user  $k$  on the subcarrier  $p$  from the BS  $b$ . Then, according to the channel model above and considering the additive white Gaussian noise (AWGN)  $\mathbf{v}_{b,k,p}$  at the receivers,  $\mathbf{y}_{b,k,p}$  can be expressed by combining (1) and (2) as

$$\begin{aligned} \mathbf{y}_{b,k,p} &= \mathbf{h}_{b,k,p}^H \mathbf{x}_{b,p} + \mathbf{v}_{b,k,p} \\ &= \left( \mathbf{H}_{b,k,p}^H + \sum_{r=1}^R \mathbf{F}_{r,k,p}^H \mathbf{\Theta}_r^H \mathbf{G}_{b,r,p} \right) \sum_{j=1}^K \mathbf{w}_{b,p,j} s_{p,j} + \mathbf{v}_{b,k,p}. \end{aligned} \quad (5)$$

Since there are  $B$  BSs serving  $K$  users simultaneously, the received signal at user  $k$  is the superposition of the signals transmitted by  $B$  BSs. Therefore, let  $\mathbf{y}_{k,p} \in \mathbb{C}^U$  denote the received signal at the user  $k$  on the subcarrier  $p$ , we have its expression as shown in (6) at the bottom of this page, where  $\mathbf{z}_{k,p} \triangleq [z_{k,p,1}^T, \dots, z_{k,p,U}^T]^T$  denotes the AWGN with zero mean  $\mathbf{0}_U$  and covariance  $\mathbf{\Xi}_{k,p} = \sigma^2 \mathbf{I}_U$ . Note that the first term on the right-hand side of (6) is the desired signal to user  $k$ , while the second term denotes the interference from other users. As there are  $P$  subcarriers available in total, we can denote the received signal at user  $k$  as  $\{\mathbf{y}_{k,p}\}_{p=1}^P$ .

#### E. Problem fomulation

Based on the system model above, we consider to maximize the WSR of the proposed RIS-aided cell-free network in this

subsection. At first, the received signal  $\mathbf{y}_{b,k,p}$  in (6) can be simplified as

$$\begin{aligned} \mathbf{y}_{k,p} &= \sum_{b=1}^B \sum_{j=1}^K \left( \mathbf{H}_{b,k,p}^H + \sum_{r=1}^R \mathbf{F}_{r,k,p}^H \mathbf{\Theta}_r^H \mathbf{G}_{b,r,p} \right) \mathbf{w}_{b,p,j} s_{p,j} + \mathbf{z}_{k,p} \\ &\stackrel{(a)}{=} \sum_{b=1}^B \sum_{j=1}^K (\mathbf{H}_{b,k,p}^H + \mathbf{F}_{k,p}^H \mathbf{\Theta}^H \mathbf{G}_{r,p}) \mathbf{w}_{b,p,j} s_{p,j} + \mathbf{z}_{k,p} \\ &\stackrel{(b)}{=} \sum_{b=1}^B \sum_{j=1}^K \mathbf{h}_{b,k,p}^H \mathbf{w}_{b,p,j} s_{p,j} + \mathbf{z}_{k,p} \\ &\stackrel{(c)}{=} \sum_{j=1}^K \mathbf{h}_{k,p}^H \mathbf{w}_{p,j} s_{p,j} + \mathbf{z}_{k,p}, \end{aligned} \quad (7)$$

where (a) holds by defining  $\mathbf{\Theta} = \text{diag}(\mathbf{\Theta}_1, \dots, \mathbf{\Theta}_R)$ ,  $\mathbf{F}_{k,p} = [\mathbf{F}_{1,k,p}^T, \dots, \mathbf{F}_{R,k,p}^T]^T$ , and  $\mathbf{G}_{r,p} = [\mathbf{G}_{1,r,p}^T, \dots, \mathbf{G}_{B,r,p}^T]^T$ , (b) holds according to (2), and (c) holds by defining  $\mathbf{h}_{k,p} = [\mathbf{h}_{1,k,p}^T, \dots, \mathbf{h}_{B,k,p}^T]^T$  and  $\mathbf{w}_{p,k} = [\mathbf{w}_{1,p,k}^T, \dots, \mathbf{w}_{B,p,k}^T]^T$ . Then, the SINR for the transmitted symbol  $s_{p,k}$  at the user  $k$  on the subcarrier  $p$  can be easily calculated as

$$\begin{aligned} \gamma_{k,p} &= \frac{\mathbf{h}_{k,p}^H \mathbf{w}_{p,k}}{\mathbf{h}_{k,p}^H \left( \sum_{j=1, j \neq k}^K \mathbf{h}_{k,p}^H \mathbf{w}_{p,j} (\mathbf{h}_{k,p}^H \mathbf{w}_{p,j})^H + \mathbf{\Xi}_{k,p} \right) \mathbf{w}_{p,k}}^{-1} \end{aligned} \quad (8)$$

Then, the WSR  $R_{\text{sum}}$  of all  $K$  users is given by

$$\begin{aligned} R_{\text{sum}} &= \sum_{k=1}^K \eta_k \sum_{p=1}^P R_{k,p} = \sum_{k=1}^K \eta_k \sum_{p=1}^P \log_2(1 + \gamma_{k,p}) \\ &= \sum_{k=1}^K \sum_{p=1}^P \eta_k \log_2(1 + \gamma_{k,p}), \end{aligned} \quad (9)$$

where  $\eta_k \in \mathbb{R}^+$  represents the weight of the user  $k$ .

We assume that each BS has its own maximum transmit power constraint, which can be written as

$$\sum_{k=1}^K \sum_{p=1}^P \|\mathbf{w}_{b,p,k}\| \leq P_{b,\max}, \quad \forall b \in \mathcal{B}, \quad (10)$$

where  $P_{b,\max}$  denotes the maximum transmit power of the BS  $b$ . Moreover, for each RIS, we have the phase shift constraint as shown in (4).

Finally, the original WSR maximization optimization problem  $\mathcal{P}^o$  to maximize the WSR (9) with the active precoding design of  $\mathbf{W}$  at the BSs and the passive precoding design of

---


$$\begin{aligned} \mathbf{y}_{k,p} &= \sum_{b=1}^B \mathbf{y}_{b,k,p} + \mathbf{z}_{k,p} = \sum_{b=1}^B \sum_{j=1}^K \left( \mathbf{H}_{b,k,p}^H + \sum_{r=1}^R \mathbf{F}_{r,k,p}^H \mathbf{\Theta}_r^H \mathbf{G}_{b,r,p} \right) \mathbf{w}_{b,p,j} s_{p,j} + \mathbf{z}_{k,p} \\ &= \underbrace{\sum_{b=1}^B \left( \mathbf{H}_{b,k,p}^H + \sum_{r=1}^R \mathbf{F}_{r,k,p}^H \mathbf{\Theta}_r^H \mathbf{G}_{b,r,p} \right) \mathbf{w}_{b,p,k} s_{p,k}}_{\text{Desired signal to user } k} + \underbrace{\sum_{b=1}^B \sum_{j=1, j \neq k}^K \left( \mathbf{H}_{b,k,p}^H + \sum_{r=1}^R \mathbf{F}_{r,k,p}^H \mathbf{\Theta}_r^H \mathbf{G}_{b,r,p} \right) \mathbf{w}_{b,p,j} s_{p,j}}_{\text{Interference from other users}} + \mathbf{z}_{k,p}. \end{aligned} \quad (6)$$

$\Theta$  at the RISs, subject to the BS power constraint (10) and RIS phase shift constraint (4) can be originally formulated as

$$\mathcal{P}^o : \max_{\Theta, \mathbf{W}} f(\Theta, \mathbf{W}) = \sum_{k=1}^K \sum_{p=1}^P \eta_k \log_2(1 + \gamma_{k,p}) \quad (11a)$$

$$\text{s.t. } C_1 : \sum_{k=1}^K \sum_{p=1}^P \|\mathbf{w}_{b,p,k}\| \leq P_{b,\max}, \quad \forall b \in \mathcal{B}, \quad (11b)$$

$$C_2 : \theta_{r,n} \in \mathcal{F}, \quad \forall r \in \mathcal{R}, \forall n \in \mathcal{N}, \quad (11c)$$

where we have defined  $\mathbf{W}$  as follows for expression simplicity:

$$\mathbf{W} = [\mathbf{w}_{1,1}^T, \mathbf{w}_{1,2}^T, \dots, \mathbf{w}_{1,K}^T, \mathbf{w}_{2,1}^T, \mathbf{w}_{2,2}^T, \dots, \mathbf{w}_{P,K}^T]^T. \quad (12)$$

However, due to the non-convex complex objective function (11a), the joint optimization of the phase shift matrix  $\Theta$  and the precoding vector  $\mathbf{W}$  is very challenging. Fortunately, inspired by the fractional programming (FP) methods designed for solving the non-convex problems [34], [35], we propose a joint precoding framework to find an approximate solution to the problem  $\mathcal{P}^o$  in (11) in the following Section III.

### III. PROPOSED JOINT PRECODING FRAMEWORK

In this section, we present the proposed joint precoding framework to solve the WSR optimization problem  $\mathcal{P}^o$  in (11). Specifically, the section is summarized as follows. An overview of the proposed framework is provided in Subsection III-A, where the problem  $\mathcal{P}^o$  in (11) is divided into three subproblems. Next, the detailed algorithms to solve these three subproblems are given in Subsections III-B, III-C, and III-D, respectively. Then, the discussions of the practical RIS reflection coefficients are given in Subsection III-E. Finally, the convergence and complexity of the proposed framework are provided in Subsection III-F.

#### A. Overview of the proposed joint precoding framework

Firstly, to deal with the complexity of sum-logarithms in the WSR maximization problem  $\mathcal{P}^o$  in (11), based on the multidimensional complex Lagrangian dual reformulation, a method has been proposed in [34] to decouple the logarithms, based on which we have the following *Proposition 1*.

**Proposition 1:** By introducing an auxiliary variable  $\rho \in \mathbb{R}^{PK}$  with  $\rho = [\rho_{1,1}, \rho_{1,2}, \dots, \rho_{1,K}, \rho_{2,1}, \rho_{2,2}, \dots, \rho_{P,K}]^T$ , the original problem  $\mathcal{P}^o$  in (11) is equivalent to

$$\begin{aligned} \bar{\mathcal{P}} : \max_{\Theta, \mathbf{W}, \rho} f(\Theta, \mathbf{W}, \rho) \\ \text{s.t. } C_1 : \sum_{k=1}^K \sum_{p=1}^P \|\mathbf{w}_{b,p,k}\| \leq P_{b,\max}, \quad \forall b \in \mathcal{B}, \quad (13) \\ C_2 : \theta_{r,n} \in \mathcal{F}, \quad \forall r \in \mathcal{R}, \forall n \in \mathcal{N}, \end{aligned}$$

where the new objective function  $f(\Theta, \mathbf{W}, \rho)$  is

$$\begin{aligned} f(\Theta, \mathbf{W}, \rho) = \sum_{k=1}^K \sum_{p=1}^P \eta_k \log_2(1 + \rho_{k,p}) - \sum_{k=1}^K \sum_{p=1}^P \eta_k \rho_{k,p} \\ + \sum_{k=1}^K \sum_{p=1}^P \eta_k (1 + \rho_{k,p}) f_{k,p}(\Theta, \mathbf{W}), \end{aligned} \quad (14)$$

#### Algorithm 1 Proposed Joint Precoding Framework.

---

**Input:** The channels  $\mathbf{H}_{b,k,p}$ ,  $\mathbf{G}_{b,r,p}$  and  $\mathbf{F}_{r,k,p}$  where  $\forall b \in \mathcal{B}, k \in \mathcal{K}, p \in \mathcal{P}$ ; user weights  $\eta_k$ ,  $\forall k \in \mathcal{K}$ .  
**Output:** Optimized active precoding vector  $\mathbf{W}$ ; Optimized passive precoding matrix  $\Theta$ ; Weighted sum-rate  $R_{\text{sum}}$ .

- 1: Initialize  $\Theta$  and  $\mathbf{W}$ ;
- 2: **while** no convergence of  $R_{\text{sum}}$  **do**
- 3:   Update  $\rho^{\text{opt}}$  by (16);
- 4:   Update  $\xi^{\text{opt}}$  by (20);
- 5:   Update  $\mathbf{W}^{\text{opt}}$  by solving (25);
- 6:   Update  $\varpi^{\text{opt}}$  by (31);
- 7:   Update  $\Theta^{\text{opt}}$  by solving (37);
- 8:   Update  $R_{\text{sum}}$  by (9);
- 9: **end while**
- 10: **return**  $\Theta$ ,  $\mathbf{W}$  and  $R_{\text{sum}}$ .

---

where the function  $f_{k,p}(\Theta, \mathbf{W})$  is denoted by

$$f_{k,p}(\Theta, \mathbf{W}) = \mathbf{w}_{p,k}^H \mathbf{h}_{k,p} \left( \sum_{j=1}^K \mathbf{h}_{k,p}^H \mathbf{w}_{p,j} (\mathbf{h}_{k,p}^H \mathbf{w}_{p,j})^H + \Xi_{k,p} \right)^{-1} \mathbf{h}_{k,p}^H \mathbf{w}_{p,k}. \quad (15)$$

*Proof:* Detailed proof of this reformulation method is given in [35]. ■

Then, we propose the joint active and passive precoding framework to optimize the variables  $\rho$ ,  $\mathbf{W}$ , and  $\Theta$  in (13) iteratively. The key idea of the framework is to fix the other two variables and optimize the remained one, e.g., fix  $(\rho, \Theta)$  and optimize  $\mathbf{W}$ . After introducing two auxiliary variables  $\xi$  and  $\varpi$ , the proposed joint precoding framework to maximize the WSR is summarized in **Algorithm 1**, where the optimal solution of  $\mathbf{X}$  is denoted by  $\mathbf{X}^{\text{opt}}$ . In this framework, the variables  $\rho$ ,  $\xi$ ,  $\mathbf{W}$ ,  $\varpi$ , and  $\Theta$  are updated iteratively, until the convergence of the objective function is achieved.

The optimal solutions to these variables in each step will be introduced in the following three subsections. Specifically, the solution to  $\rho^{\text{opt}}$  is firstly present in Subsection III-B. Then, the solutions to  $\xi^{\text{opt}}$  and  $\mathbf{W}^{\text{opt}}$  for the active precoding design are provided in Subsection III-C. After that, the solutions to  $\varpi^{\text{opt}}$  and  $\Theta^{\text{opt}}$  for the passive precoding design are finally discussed in Subsection III-D.

#### B. Fix $(\Theta, \mathbf{W})$ and solve $\rho^{\text{opt}}$

Given fixed  $(\Theta^*, \mathbf{W}^*)$ , the optimal  $\rho$  in (14) can be obtained by solving  $\partial f / \partial \rho_{k,p} = 0$  for  $\forall k \in \mathcal{K}, \forall p \in \mathcal{P}$ . The solution can be written as

$$\rho_{k,p}^{\text{opt}} = \gamma_{k,p}, \quad \forall k \in \mathcal{K}, \forall p \in \mathcal{P}. \quad (16)$$

By substituting  $\rho_{k,p}^{\text{opt}}$  in (16) back in  $f$  in (14), one can notice that, only the last term in (14) is associated with the variables  $\mathbf{W}$  and  $\Theta$ . Hence, the objective function  $f$  in (14) can be further simplified and solved as shown in the following two subsections.

C. Active precoding: fix  $(\Theta, \rho)$  and solve  $\mathbf{W}^{\text{opt}}$

In the case of given  $(\Theta^*, \rho^*)$ , the equivalent WSR maximization problem  $\bar{\mathcal{P}}$  in (13) can be reformulated as the following subproblem  $\mathcal{P}_{\text{active}}$  for the active precoding design at BSs:

$$\begin{aligned} \mathcal{P}_{\text{active}} : \max_{\mathbf{W}} \quad & g_1(\mathbf{W}) = \sum_{k=1}^K \sum_{p=1}^P \mu_{k,p} f_{k,p}(\Theta^*, \mathbf{W}) \\ \text{s.t. } \quad & C_1 : \sum_{k=1}^K \sum_{p=1}^P \|\mathbf{w}_{b,p,k}\| \leq P_{b,\max}, \quad \forall b \in \mathcal{B}, \end{aligned} \quad (17)$$

where  $\mu_{k,p} = \eta_k(1 + \rho_{k,p}^*)$  holds. Notice that the reformulated subproblem  $\mathcal{P}_{\text{active}}$  in (17) is still too difficult to solve due to the complexity of matrix inversion in  $f_{k,p}$  in (15). Actually, this subproblem is a multi-variable sum-of-ratios problem, which has been discussed in [34]. Inspired by the methods proposed in [34], here we can utilize the multidimensional complex quadratic transform to reformulate this subproblem, and then we obtain *Proposition 2* as below.

**Proposition 2:** With multidimensional complex quadratic transform, by introducing auxiliary variables  $\xi_{p,k} \in \mathbb{C}^U$  and  $\xi = [\xi_{1,1}, \xi_{1,2}, \dots, \xi_{1,K}, \xi_{2,1}, \xi_{2,2}, \dots, \xi_{P,K}]$ , the subproblem  $\mathcal{P}_{\text{active}}$  in (17) can be further reformulated as

$$\begin{aligned} \bar{\mathcal{P}}_{\text{active}} : \max_{\mathbf{W}, \xi} \quad & g_2(\mathbf{W}, \xi) \\ \text{s.t. } \quad & C_1 : \sum_{k=1}^K \sum_{p=1}^P \|\mathbf{w}_{b,p,k}\| \leq P_{b,\max}, \quad \forall b \in \mathcal{B}, \end{aligned} \quad (18)$$

where

$$\begin{aligned} g_2(\mathbf{W}, \xi) = & \sum_{k=1}^K \sum_{p=1}^P 2\sqrt{\mu_{k,p}} \Re \{ \xi_{k,p}^H \mathbf{h}_{k,p}^H \mathbf{w}_{p,k} \} \\ & - \sum_{k=1}^K \sum_{p=1}^P \xi_{k,p}^H \left( \sum_{j=1}^K \mathbf{h}_{k,p}^H \mathbf{w}_{p,j} (\mathbf{h}_{k,p}^H \mathbf{w}_{p,j})^H + \Xi_{k,p} \right) \xi_{k,p}. \end{aligned} \quad (19)$$

*Proof:* Detailed proof of this transform method is given in [35]. ■

Therefore, we can optimize the variables  $\mathbf{W}$  and  $\xi$  in (18) alternatively. The reformulated subproblem  $\bar{\mathcal{P}}_{\text{active}}$  in (18) can be further divided into two subproblems and respectively solved as follows.

1) Fix  $\mathbf{W}$  and solve  $\xi^{\text{opt}}$ : While fixing  $\mathbf{W}$  in  $\bar{\mathcal{P}}_{\text{active}}$  in (18), by setting  $\partial g_2 / \partial \xi_{k,p}$  to zero, the optimal  $\xi$  can be obtained by

$$\begin{aligned} \xi_{k,p}^{\text{opt}} = & \sqrt{\mu_{k,p}} \left( \sum_{j=1}^K \mathbf{h}_{k,p}^H \mathbf{w}_{p,j} (\mathbf{h}_{k,p}^H \mathbf{w}_{p,j})^H + \Xi_{k,p} \right)^{-1} \mathbf{h}_{k,p}^H \mathbf{w}_{p,j}, \\ & \forall k \in \mathcal{K}, \forall p \in \mathcal{P}. \end{aligned} \quad (20)$$

2) Fix  $\xi$  and solve  $\mathbf{W}^{\text{opt}}$ : While fixing  $\xi$  in  $\bar{\mathcal{P}}_{\text{active}}$  in (18), for simplification and clarity of (18), we can first define

$$\mathbf{a}_p = \sum_{k=1}^K \mathbf{h}_{k,p} \xi_{k,p} \xi_{k,p}^H \mathbf{h}_{k,p}^H, \quad (21a)$$

$$\mathbf{A}_p = \mathbf{I}_K \otimes \mathbf{a}_p, \quad (21b)$$

$$v_{k,p} = \xi_{k,p}^H \mathbf{h}_{k,p}^H \mathbf{w}_{p,k}. \quad (21c)$$

Then, by substituting (21) into  $g_2$  in (19), we can rewritten  $g_2$  as

$$g_3(\mathbf{W}) = -\mathbf{W}^H \mathbf{A} \mathbf{W} + \Re \{ 2\mathbf{V}^H \mathbf{W} \} - Y, \quad (22)$$

where

$$\mathbf{A} = \begin{bmatrix} \mathbf{A}_1 & & \\ & \ddots & \\ & & \mathbf{A}_P \end{bmatrix}, \quad (23a)$$

$$\mathbf{V} = [v_{1,1}, v_{1,2}, \dots, v_{1,K}, v_{2,1}, v_{2,2}, \dots, v_{P,K}]^T, \quad (23b)$$

$$Y = \sum_{k=1}^K \sum_{p=1}^P \xi_{k,p}^H \Xi_{k,p} \xi_{k,p}. \quad (23c)$$

Next, For further clarity, we consider to simplify the constraint  $C_1$  in (18), and we can obtain the following *Lemma 1* as follows.

**Lemma 1:** The constraint  $C_1$  in (18) can be rewritten as

$$\mathbf{W}^H \mathbf{D}_b \mathbf{W} \leq P_{b,\max}, \quad \forall b \in \mathcal{B}, \quad (24)$$

where  $\mathbf{D}_b = \mathbf{I}_{PK} \otimes \{(\mathbf{e}_b \mathbf{e}_b^H) \otimes \mathbf{I}_M\}$  and  $\mathbf{e}_b \in \mathbb{R}^B$ .

*Proof:* See Appendix A. ■

Therefore, by using (22) and (24), the active precoding problem  $\bar{\mathcal{P}}_{\text{active}}$  in (18) can be further simplified as

$$\begin{aligned} \hat{\mathcal{P}}_{\text{active}} : \max_{\mathbf{W}} \quad & g_3(\mathbf{W}) = -\mathbf{W}^H \mathbf{A} \mathbf{W} + \Re \{ 2\mathbf{V}^H \mathbf{W} \} - Y \\ \text{s.t. } \quad & C_1 : \mathbf{W}^H \mathbf{D}_b \mathbf{W} \leq P_{b,\max}, \quad \forall b \in \mathcal{B}. \end{aligned} \quad (25)$$

Finally, notice that since the matrices  $\mathbf{A}$  and  $\mathbf{D}_b, \forall b \in \mathcal{B}$  are all positive semidefinite, the simplified subproblem  $\hat{\mathcal{P}}_{\text{active}}$  in (25) is a standard QCQP problem, which can be directly solved by the standard convex tools such as CVX [42]. We also give a feasible solution to obtain  $\mathbf{W}^{\text{opt}}$  in Appendix B.

D. Passive precoding: fix  $(\rho, \mathbf{W})$  and solve  $\Theta^{\text{opt}}$

Based on the given  $(\rho^*, \mathbf{W}^*)$ , for the equivalent WSR maximization problem  $\bar{\mathcal{P}}$  in (13), the subproblem of the passive precoding design at RISs can be equivalently written as

$$\begin{aligned} \mathcal{P}_{\text{passive}} : \max_{\Theta} \quad & g_4(\Theta) = \sum_{k=1}^K \sum_{p=1}^P \mu_{k,p} f_{k,p}(\Theta, \mathbf{W}^*) \\ \text{s.t. } \quad & C_2 : \theta_{r,n} \in \mathcal{F}, \quad \forall r \in \mathcal{R}, \forall n \in \mathcal{N}, \end{aligned} \quad (26)$$

where  $\mu_{k,p} = \eta_k(1 + \rho_{k,p}^*)$ . Similarly, to reduce the complexity, we wish to simplify the expression of  $g_4$  in (26). Firstly, by defining a new auxiliary function with respect to  $\Theta$  as

$$\mathbf{Q}_{k,p,j}(\Theta) = \sum_{b=1}^B (\mathbf{H}_{b,k,p}^H + \mathbf{F}_{k,p}^H \Theta^H \mathbf{G}_{b,p}) \mathbf{w}_{b,p,j}, \quad (28)$$

we can rewrite  $g_4$  in (26) as (27) at the bottom of this page. However, this subproblem is still hard to solve due to matrix inversion in  $f_{k,p}$  in (15). Again, we consider to exploit the multidimensional complex quadratic transform [34] to address this issue by using the following *Proposition 3*.

**Proposition 3:** With multidimensional complex quadratic transform, by introducing an auxiliary variable  $\varpi_{p,k} \in \mathbb{C}^U$  and  $\varpi = [\varpi_{1,1}, \varpi_{1,2}, \dots, \varpi_{1,K}, \varpi_{2,1}, \varpi_{2,2}, \dots, \varpi_{P,K}]$ , the passive precoding subproblem  $\mathcal{P}_{\text{passive}}$  in (26) can be reformulated as

$$\bar{\mathcal{P}}_{\text{passive}} : \max_{\Theta} g_5(\Theta, \varpi) = \sum_{k=1}^K \sum_{p=1}^P g_{k,p}(\Theta, \varpi) \quad (29a)$$

$$\text{s.t. } C_2 : \theta_{r,n} \in \mathcal{F}, \forall r \in \mathcal{R}, \forall n \in \mathcal{N}, \quad (29b)$$

where

$$g_{k,p}(\Theta, \varpi) = 2\sqrt{\mu_{k,p}} \Re \{ \varpi_{k,p}^H \mathbf{Q}_{k,p,k}(\Theta) \} - \varpi_{k,p}^H \left( \sum_{j=1}^K \mathbf{Q}_{k,p,j}(\Theta) \mathbf{Q}_{k,p,j}^H(\Theta) + \Xi_{k,p} \right) \varpi_{k,p}. \quad (30)$$

*Proof:* Detailed constructive proof of this reformulation method is given in [35]. ■

Next, similar to the previous processing of the subproblem  $\bar{\mathcal{P}}_{\text{active}}$  in (18), we consider to optimize two variables  $\Theta$  and  $\varpi$  in (29) alternatively. The reformulated subproblem  $\bar{\mathcal{P}}_{\text{passive}}$  in (29) can be further divided into two subproblems and respectively solved as follows.

1) *Fix  $\Theta$  and solve  $\varpi^{\text{opt}}$ :* For given fixed  $\Theta^*$  in  $\bar{\mathcal{P}}_{\text{passive}}$  in (29), by solving  $\partial g_5 / \partial \varpi_{k,p} = 0$  for  $\forall k \in \mathcal{K}$  and  $\forall p \in \mathcal{P}$ , we can obtain the optimal  $\varpi$  by

$$\varpi_{k,p}^{\text{opt}} = \sqrt{\mu_{k,p}} \left( \sum_{j=1}^K \mathbf{Q}_{k,p,j}(\Theta^*) \mathbf{Q}_{k,p,j}^H(\Theta^*) + \Xi_{k,p} \right)^{-1} \mathbf{Q}_{k,p,j}(\Theta^*), \quad \forall k \in \mathcal{K}, \forall p \in \mathcal{P}. \quad (31)$$

2) *Fix  $\varpi$  and solve  $\Theta^{\text{opt}}$ :* While fixing  $\varpi$  in  $g_5$  in (29), due to the complexity of  $\bar{\mathcal{P}}_{\text{passive}}$  in (29), we first consider to simplify the expression of  $g_5$  by using the new auxiliary function  $\mathbf{Q}_{k,p,j}(\Theta)$  with respect to  $\Theta$  in (28) as follows:

$$\begin{aligned} & \varpi_{k,p}^H \mathbf{Q}_{k,p,j}(\Theta) \\ & \stackrel{(a)}{=} \sum_{b=1}^B (\varpi_{k,p}^H \mathbf{H}_{b,k,p}^H \mathbf{w}_{b,p,j} + \varpi_{k,p}^H \mathbf{F}_{k,p}^H \Theta^H \mathbf{G}_{b,p} \mathbf{w}_{b,p,j}) \\ & \stackrel{(b)}{=} \sum_{b=1}^B \varpi_{k,p}^H \mathbf{H}_{b,k,p}^H \mathbf{w}_{b,p,j} + \theta^H \sum_{b=1}^B \text{diag}(\varpi_{k,p}^H \mathbf{F}_{k,p}^H) \mathbf{G}_{b,p} \mathbf{w}_{b,p,j} \\ & \stackrel{(c)}{=} c_{k,p,j} + \theta^H \mathbf{g}_{k,p,j}, \end{aligned} \quad (32)$$

where (a) holds according to (27), (b) is obtained by defining  $\theta = \Theta \mathbf{1}_{RN}$ , and (c) is achieved by defining

$$c_{k,p,j} = \sum_{b=1}^B \varpi_{k,p}^H \mathbf{H}_{b,k,p}^H \mathbf{w}_{b,p,j}, \quad (33a)$$

$$\mathbf{g}_{k,p,j} = \sum_{b=1}^B \text{diag}(\varpi_{k,p}^H \mathbf{F}_{k,p}^H) \mathbf{G}_{b,p} \mathbf{w}_{b,p,j}. \quad (33b)$$

By substituting (32) into (30), we can obtain:

$$\begin{aligned} g_{k,p}(\Theta) &= 2\sqrt{\mu_{k,p}} \Re \{ c_{k,p,k} + \theta^H \mathbf{g}_{k,p,k} \} \\ &\quad - \sum_{j=1}^K (c_{k,p,j} + \theta^H \mathbf{g}_{k,p,j}) (c_{k,p,j}^* + \mathbf{g}_{k,p,j}^H \theta) - \varpi_{k,p}^H \Xi_{k,p} \varpi_{k,p}. \end{aligned} \quad (34)$$

Then, we can further substitute (34) into (29a), so that  $g_5$  in (29a) can be rewritten as

$$g_6(\Theta) = -\theta^H \Lambda \theta + \Re \{ 2\theta^H \nu \} - \zeta, \quad (35)$$

where

$$\Lambda = \sum_{k=1}^K \sum_{p=1}^P \sum_{j=1}^K \mathbf{g}_{k,p,j} \mathbf{g}_{k,p,j}^H, \quad (36a)$$

$$\nu = \sum_{k=1}^K \sum_{p=1}^P \sqrt{\mu_{k,p}} \mathbf{g}_{k,p,k} - \sum_{k=1}^K \sum_{p=1}^P \sum_{j=1}^K c_{k,p,j}^* \mathbf{g}_{k,p,j}, \quad (36b)$$

$$\zeta = \sum_{k=1}^K \sum_{p=1}^P \sum_{j=1}^K |c_{k,p,j}|^2 + \sum_{k=1}^K \sum_{p=1}^P \varpi_{k,p}^H \Xi_{k,p} \varpi_{k,p} \quad (36c)$$

$$- 2 \sum_{k=1}^K \sum_{p=1}^P \sqrt{\mu_{k,p}} \Re \{ c_{k,p,k} \}. \quad (36d)$$

Therefore, the reformulated passive precoding subproblem  $\bar{\mathcal{P}}_{\text{passive}}$  in (29) can be further simplified as

$$\begin{aligned} \hat{\mathcal{P}}_{\text{passive}} : \max_{\Theta} g_6(\Theta) &= -\theta^H \Lambda \theta + \Re \{ 2\theta^H \nu \} - \zeta \\ \text{s.t. } C_2 : \theta_{r,j} &\in \mathcal{F}, \forall r \in \mathcal{R}, \forall j \in \mathcal{N}. \end{aligned} \quad (37)$$

This simplified subproblem  $\hat{\mathcal{P}}_{\text{passive}}$  is similar to those in [41], [43], [44]. Obviously, since the matrix  $\Lambda$  is positive semidefinite, the objective function is convex. Besides, since we have  $\mathcal{F} \triangleq \{ \theta_{r,j} \mid |\theta_{r,j}| \leq 1 \}$  according to (4), the constraint  $C_2$  is also convex. Therefore,  $\Theta^{\text{opt}}$  can be directly obtained by the standard convex tools such as CVX [42]. Again, we also give a feasible solution to  $\bar{\mathcal{P}}_{\text{passive}}$  in Appendix C.

#### E. Extension to non-ideal RIS cases

Up to now, we have provided a complete joint precoding framework for the proposed RIS-aided cell-free network, where ideal RIS case as mentioned in Subsection II-C is considered. In this subsection, we will extend this framework to the more practical non-ideal RIS cases.

$$g_4(\Theta) = \sum_{k=1}^K \sum_{p=1}^P \sqrt{\mu_{k,p}} \mathbf{Q}_{k,p,k}^H(\Theta) \left( \sum_{j=1}^K \mathbf{Q}_{k,p,j}(\Theta) \mathbf{Q}_{k,p,j}^H(\Theta) + \Xi_{k,p} \right)^{-1} \mathbf{Q}_{k,p,k}(\Theta). \quad (27)$$

1) *Non-ideal RIS cases*: According to (4) in Subsection II-C,  $\mathcal{F}$  is defined as the ideal RIS case, where both the amplitude and phase of  $\theta_{r,j}$  associated with the RIS element can be controlled independently and continuously. However, limited by the hardware implementation of metamaterials, the RISs in practice are usually non-ideal. For consistent discussion, here we redefine the ideal RIS case  $\mathcal{F}$  as  $\mathcal{F}_1$ . We also define  $\mathcal{F}_2$  as the general case where only the phase of  $\theta_{r,j}$  can be controlled continuously, and  $\mathcal{F}_3$  as the practical case where the low-resolution phase of  $\theta_{r,n}$  is discrete [23], i.e.,

$$\mathcal{F}_1 \triangleq \left\{ \theta_{r,n} \mid |\theta_{r,n}| \leq 1 \right\}, \quad (38a)$$

$$\mathcal{F}_2 \triangleq \left\{ \theta_{r,n} \mid |\theta_{r,n}| = 1 \right\}, \quad (38b)$$

$$\mathcal{F}_3 \triangleq \left\{ \theta_{r,n} \mid \theta_{r,n} \in \left\{ 1, e^{j\frac{2\pi}{L}}, \dots, e^{j\frac{2\pi(L-1)}{L}} \right\} \right\}, \quad (38c)$$

where  $L$  indicates that  $\mathcal{F}_3$  contains  $L$  discrete phase shifts.

2) *Approximation in non-ideal RIS cases*: According to the simplified subproblem  $\hat{\mathcal{P}}_{\text{passive}}$  in (37), for the passive precoding design at the RISs, when the phase shift constraint  $\mathcal{F}$  is  $\mathcal{F}_1$  as discussed above, the subproblem  $\hat{\mathcal{P}}_{\text{passive}}$  can be directly solved due to the convexity of  $\mathcal{F}_1$ .

However, when the constraint  $\mathcal{F}$  in (37) is  $\mathcal{F}_2$  or  $\mathcal{F}_3$ , the simplified subproblem  $\hat{\mathcal{P}}_{\text{passive}}$  in (37) becomes non-convex. The common solution to address such problem is to relax the constraint of the phase shift matrix in  $\mathcal{F}_2$  or  $\mathcal{F}_3$  [41], [43]. Hence, by introducing an auxiliary variable  $\tilde{\Theta}$ , the simplified subproblem  $\hat{\mathcal{P}}_{\text{passive}}$  in (37) can be relaxed as

$$\begin{aligned} \hat{\mathcal{P}}_{\text{passive-relaxed}} : \max_{\tilde{\Theta}} \quad & g_7(\tilde{\Theta}) = -\tilde{\Theta}^H \Lambda \tilde{\Theta} + \Re \left\{ 2\tilde{\Theta}^H \nu \right\} - \zeta \\ \text{s.t.} \quad & C_2 : \tilde{\theta}_{r,j} \in \mathcal{F}_1, \forall r \in \mathcal{R}, \forall j \in \mathcal{N}. \end{aligned} \quad (39)$$

This relaxed subproblem  $\hat{\mathcal{P}}_{\text{passive-relaxed}}$  is convex, which is now similar to the subproblem  $\hat{\mathcal{P}}_{\text{passive}}$  in (37). Thus,  $\tilde{\Theta}^{\text{opt}}$  can be directly solved by the standard convex tools such as CVX [42] as well. Then, based on the proximity principle, we can map the solved  $\tilde{\Theta}^{\text{opt}}$  to the elements in  $\mathcal{F}_2$  or  $\mathcal{F}_3$  by a quantization operation, which is common in existing works [22], [26], [43], and can be written as

$$\begin{cases} |\theta_{r,j}^{\text{sub}}| = 1, \\ \angle \theta_{r,j}^{\text{sub}} = \underset{\phi \in \mathcal{F}_2 \text{ or } \mathcal{F}_3}{\text{argmin}} \left| \angle \tilde{\theta}_{r,j}^{\text{opt}} - \phi \right|, \quad \forall r \in \mathcal{R}, \forall j \in \mathcal{N}, \end{cases} \quad (40)$$

where  $\theta_{r,j}^{\text{sub}}$  denotes the approximated sub-optimal solution to  $\theta_{r,j}$ . Thus, we can finally obtain  $\Theta^{\text{sub}}$  by using the approximation (40) above.

With the approximation in (40), the proposed joint precoding framework can be also used in non-ideal RIS cases  $\mathcal{F}_2$  and  $\mathcal{F}_3$  as well. It should be pointed out that, since the loss caused by the approximation might be large and hard to estimate, some other discrete optimization methods such as adaptive cross-entropy (ACE) algorithm [45] might be used to alleviate the approximation loss in the non-ideal RIS cases, which is left for future work.

## F. Convergence and complexity

1) *Convergence*: In the ideal case when  $\mathcal{F} = \mathcal{F}_1$ , the proposed joint precoding framework has strict convergence, since each step of the iteration, i.e., (16), (20), (25), (31) and (37), can be easily proved to be monotonous. However, In the non-ideal cases when  $\mathcal{F} = \mathcal{F}_2$  and  $\mathcal{F} = \mathcal{F}_3$ , the convergence of the proposed framework can not be proved strictly, since the update of  $\Theta$  has no guarantee of monotony in some cases due to the approximation operation in (40). Fortunately, the rest of iterative steps are all monotonous, so the loss caused by the approximation operation has little adverse effect on the global convergence, which will be verified by simulation results in the next Section IV.

2) *Complexity*: The overall complexity of the proposed joint precoding framework is mainly introduced by the update of the variables  $\rho$ ,  $\xi$ ,  $\mathbf{W}$ ,  $\varpi$ , and  $\Theta$ , as shown in (16), (20), (25), (31) and (37), respectively. Notice that the optimal solutions to  $\rho$ ,  $\xi$ , and  $\varpi$  are all in closed-form, which has lower complexity than those to  $\mathbf{W}$  and  $\Theta$ , since the optimal  $\mathbf{W}$  and  $\Theta$  have to be obtained iteratively. Specifically, the computational complexities of  $\rho$ ,  $\xi$ , and  $\varpi$  are mainly caused by the matrix inversion in (15), (20), and (31), respectively. The dimensions of these three matrices are all  $U$ , i.e., the number of user antennas, so the complexity is  $\mathcal{O}(U^3)$ . The computational complexities of  $\mathbf{W}$  and  $\Theta$  mainly comes from the subproblems in (25) and (37), and they are strictly related to the dimensions of the variables to be optimized. The dimension of  $\mathbf{W}$  is  $BMPK$ , while that of  $\Theta$  is  $RN$ . Thanks to the sparsity of the matrices  $\mathbf{A}$  and  $\Lambda$ , and since the subproblems  $\hat{\mathcal{P}}_{\text{active}}$  in (25) and  $\hat{\mathcal{P}}_{\text{passive}}$  in (37) are standard QCQP problems, the complexities of solving them are acceptable.

**Remark 1:** Different from the prior works, in which only some of the system parameters such as the number of RISs are multiple, our proposed RIS-aided cell-free network is the first one to simultaneously consider multiple antennas, multiple BSs, multiple users, multiple RISs and multiple subcarriers. It indicates that most of the prior discussed scenarios [15], [18], [19], [26], [41], [43], are our special cases. Moreover, by simply setting  $M$ ,  $U$ ,  $N$ ,  $B$ ,  $R$ ,  $K$ ,  $P$  to the required values in these special cases, our proposed joint precoding framework can serve as a general solution to maximize the WSR in these special cases. For instance, by setting  $B = 1$ ,  $P = 1$ , and  $R = 1$ , the proposed framework can be used to solve the WSR maximization problem in a single-carrier scenario where one BS assisted by one RIS is deployed to serve multiple users as discussed in [43].

## IV. SIMULATION RESULTS

In this section, we provided extensive simulation results under different conditions to validate the performance of the proposed concept of RIS-aided cell-free network and the corresponding joint precoding framework.

### A. Simulation setup

For the simulation of the proposed RIS-aided cell-free network, the number of antennas at each BS is set as  $M = 8$



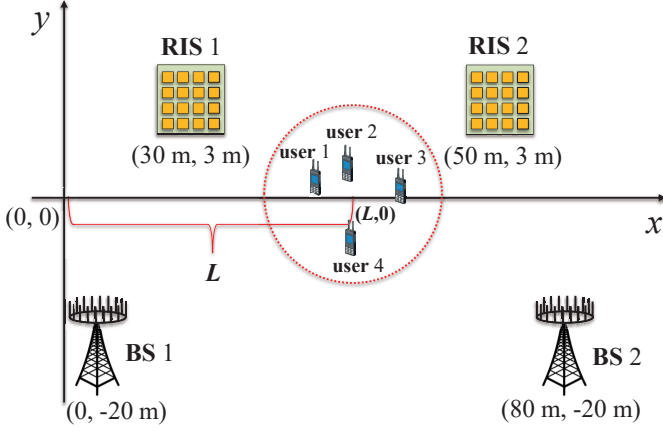


Fig. 3. The simulated scenario where two BSs assisted by two RISs serve four users.

and that at each user is set as  $U = 2$ . The number of RIS elements is set as  $N = 32$ . The number of subcarriers is set as  $P = 6$ , and the noise power is set as  $\sigma^2 = -120$  dBm.

For the channel model, firstly we consider a large-scale fading model according to [46], where the BS-RIS-user link suffers the double-fading effect discussed in [47]. Therefore, let  $d_{Bu}$ ,  $d_{BR}$ ,  $d_{Ru}$  denote the distance between BS and user, BS and RIS, RIS and user, respectively, the distance-dependent path loss of the BS-user link can be written as

$$f_d(d_{Bu}) = C_d G_B G_u d_{Bu}^{-\kappa_{Bu}}, \quad (41)$$

and that of the BS-RIS-user link can be written as

$$f_r(d_{BR}, d_{Ru}) = C_r G_B G_u d_{BR}^{-\kappa_{BR}} d_{Ru}^{-\kappa_{Ru}}, \quad (42)$$

where  $C_d$  and  $C_r$  are the channel fading variables related to the wavelength, channel status, and angle of departure (AOD), and  $C_r$  is also related to the angle of arrival (AOA), the material and size of RIS element [46];  $G_B$  and  $G_u$  denote the antenna gain of the BSs and users, respectively, and here we assume  $C_d G_B G_u = -30$  dB and  $C_r G_B G_u = -40$  dB [43];  $\kappa$  denotes the path loss exponent, and the path loss exponents of the BS-RIS link, RIS-user link, and BS-user link are set as  $\kappa_{BR} = 2$ ,  $\kappa_{Ru} = 2$ , and  $\kappa_{Bu} = 3$  [46], respectively.

Then, to account for the small-scale fading, we further consider a Rician fading channel model, thus the BS-user channel  $\mathbf{H}$  is obtained by

$$\mathbf{H} = \sqrt{\frac{\beta_{Bu}}{1 + \beta_{Bu}}} \mathbf{H}^{\text{LoS}} + \sqrt{\frac{1}{1 + \beta_{Bu}}} \mathbf{H}^{\text{NLoS}}, \quad (43)$$

where  $\beta_{Bu}$  denotes the Rician factor, and  $\mathbf{H}^{\text{LoS}}$  and  $\mathbf{H}^{\text{NLoS}}$  denote the LoS and Rayleigh fading components, respectively. Note that  $\mathbf{H}$  is equivalent to a LoS channel when  $\beta_{Bu} \rightarrow \infty$ , and a Rayleigh fading channel when  $\beta_{Bu} = 0$ . Then,  $\mathbf{H}$  is multiplied by the square root of the distance-dependent path loss  $f_d(d_{Bu})$  in (41). Similarly, the BS-RIS and RIS-user channels can also be generated by the above procedure, and let  $\beta_{BR}$  and  $\beta_{Ru}$  denote the Rician factors of them, respectively. Here we assume  $\beta_{BR} \rightarrow \infty$ ,  $\beta_{Bu} = 0$  and,  $\beta_{Ru} = 0$  [41].

At last, for the joint precoding framework, we set the weights of users as  $\eta_k = 1$ , and we assume that the channel

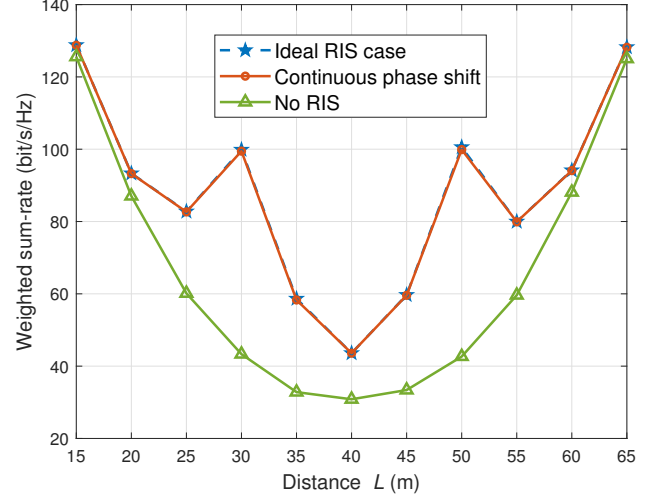


Fig. 4. Weighted sum-rate against the distance  $L$ .

state information (CSI) is perfectly known<sup>2</sup>. As an alternating algorithm,  $\Theta$  is initialized by random values in  $\mathcal{F}$ , and  $\mathbf{W}$  is initialized by identical power and random phases.

#### B. Weighted sum-rate performance of the RIS-aided cell-free network

The WSR of the proposed RIS-aided cell-free network is evaluated in this subsection. For simplicity but without loss of generality, we consider a RIS-aided cell-free system with the topology as shown in Fig. 3, where two BSs and two RISs are located at  $(0, -20\text{ m})$ ,  $(80\text{ m}, -20\text{ m})$ ,  $(30\text{ m}, 3\text{ m})$  and  $(50\text{ m}, 3\text{ m})$ , respectively, and four users are randomly distributed in a circle centered at  $(L, 0)$  with radius 1 m, where  $L$  denotes the horizontal distance between the BS 1 and the circle centre. The maximum transmit power at the BS is set as  $P_{b,\max} = 0$  dB.

Fig. 4 shows the WSR against the distance  $L$ , where the conventional cell-free network without RIS (which is denote by No RIS) is considered as benchmark to be compared with the proposed RIS-aided cell-free network. Specifically, the Ideal RIS case means that both the amplitude and phase of RIS elements can be controlled continuously and independently, i.e.,  $\mathcal{F} = \mathcal{F}_1$ , while Continuous phase shift denotes the non-ideal case  $\mathcal{F} = \mathcal{F}_2$ . More discussions about the non-ideal RIS cases will be provided in Fig. 5 and Fig. 10 later. For the conventional cell-free network without RIS, the WSR maximization problem can be rewritten as

$$\begin{aligned} \mathcal{P}_{\text{no-RIS}}^o : \quad & \max_{\mathbf{W}} f_0(\mathbf{W}) = \sum_{k=1}^K \sum_{p=1}^P \eta_k \log_2 (1 + \gamma_{k,p}^o) \\ \text{s.t. } & C_1 : \sum_{k=1}^K \sum_{p=1}^P \|\mathbf{w}_{b,p,k}\| \leq P_{b,\max}, \quad \forall b \in \mathcal{B}, \end{aligned} \quad (44)$$

<sup>2</sup>In this paper, the CSI is assumed to be perfectly known, while the challenging problem of channel estimation [21] is left for future work.

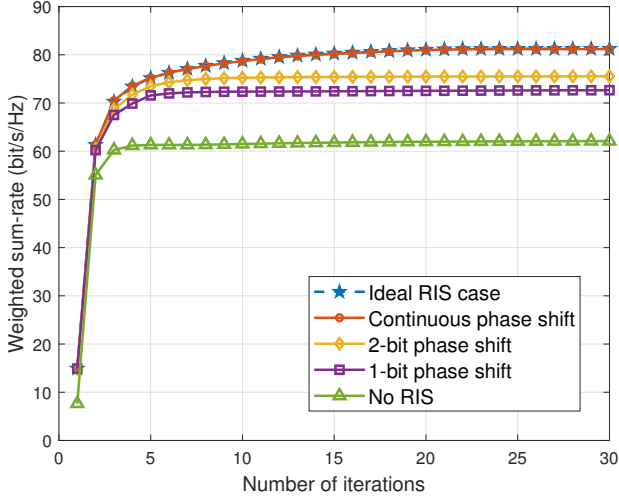


Fig. 5. Weighted sum-rate against the number of iterations.

where

$$\gamma_{k,p}^o = \mathbf{w}_{p,k}^H \mathbf{H}_{k,p} \left( \sum_{j=1, j \neq k}^K \mathbf{H}_{k,p}^H \mathbf{w}_{p,j} (\mathbf{H}_{k,p}^H \mathbf{w}_{p,j})^H + \Xi_{k,p} \right)^{-1} \mathbf{H}_{k,p}^H \mathbf{w}_{p,k}. \quad (45)$$

Obviously, the problem  $\mathcal{P}_{\text{no-RIS}}^o$  in (44) is a special case of our problem  $\mathcal{P}^o$  in (11) for the RIS-aided cell-free network. However, to the best of our knowledge, the WSR maximization problem  $\mathcal{P}_{\text{no-RIS}}^o$ , which is subject to the power constraints in the wideband cell-free system, has not been investigated in the literature. Thus, the performance curve named No RIS is achieved by the proposed joint precoding framework by simply setting the number of RISs as  $R = 0$ .

We have two observations from Fig. 4. First, as the users move away from the BSs, the WSR of the users decreases rapidly due to the signal attenuation in the conventional cell-free network. However, for the proposed RIS-aided cell-free network, we can see two obvious peaks at  $L = 30\text{ m}$  and  $L = 50\text{ m}$ , which indicates that the WSR rises when the users approach one of the two RISs, since the users can receive strong signals reflected from the RISs. For the conventional scheme without RIS, these two peaks will not appear. Thus, we can conclude that the network capacity can be substantially increased by deploying RISs in the network, and the signal coverage can be accordingly extended. Second, we can find that the curves Ideal RIS case and Continuous phase shift are very close to each other. It indicates that, for practical hardware implementation, there is no need to design amplitude-controllable RISs, since the continuous phase shift can approach the best performance in the ideal case.

### C. Convergence of the joint precoding framework

We present the convergence of the proposed algorithm by plotting the WSR against the number of iterations in Fig. 5. The simulation parameters and the network topology are same as those used in IV-B, and we fix the distance  $L$  as  $L = 25\text{ m}$ .

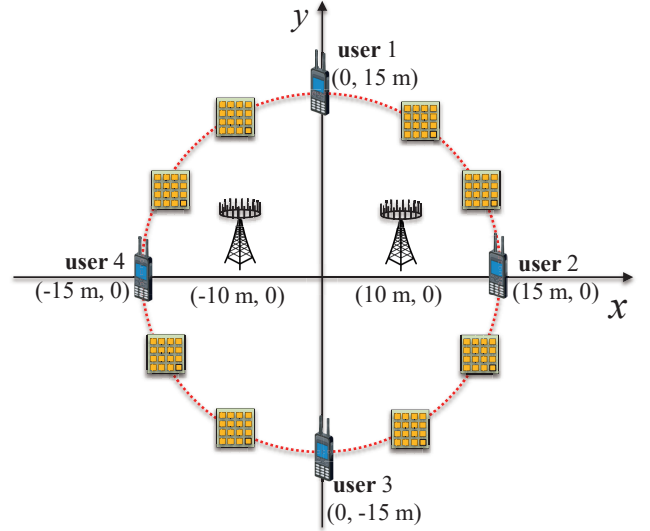


Fig. 6. The simulation scenario where two BSs and eight RISs serve four users.

To show the convergence in non-ideal low-resolution phase shift cases, we add the curves 1-bit phase shift and 2-bit phase shift to denote the case  $\mathcal{F} = \mathcal{F}_3$ , where the discrete available phase shift sets are  $\{0, \pi\}$  and  $\{0, \pi/2, \pi, 3\pi/2\}$ , respectively. The results in Fig. 5 clearly illustrate that, when the convergence error is no more than 2%, the proposed joint precoding framework can converge within 15 iterations. To be more specific, the ideal RIS case and continuous phase shift case can converge within 15 iterations. The discrete phase shift case can converge within 10 iterations. Since the conventional cell-free network without RIS does not need to address the passive precoding design at RISs, the WSR in the case No RIS converges within 8 iterations. The results indicate that, although the approximation operation in (40) causes the uncertainty of convergence, the proposed framework still enjoys the global convergence and a fast convergence speed. Besides, we can also notice that, the low-resolution phase shifts only suffer from an acceptable performance loss. For example, after 15 iterations, the WSR in Ideal RIS case is about 82 bit/s/Hz, while that of the cases 2-bit phase shift is about 75 bit/s/Hz, which suffers a loss about 8% of the ideal case. Considering the hardware implementation of RIS [23], since the low-resolution phase shift is much easier for implementation than the continuous one, this result is very encouraging for the massive deployment of RIS in the RIS-aided cell-free network.

### D. The impact of key system parameters

To reveal more design insights of the proposed RIS-aided cell-free network with different system parameters, we consider a new simulation setup as shown in Fig. 6 in this subsection, where eight RISs and two users are uniformly distributed along a circle of radius 15 m. Two BSs are located at  $(-10\text{ m}, 0)$  and  $(10\text{ m}, 0)$ , respectively. The BS maximum transmit power is set as  $P_{b,\text{max}} = -10\text{ dB}$ .

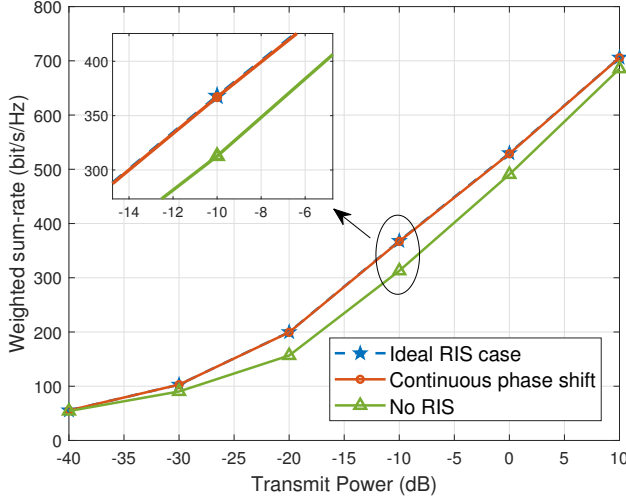


Fig. 7. Weighted sum-rate against the BS transmit power.

1) *Weighted sum-rate against BS transmit power:* To analyze the effect of BS transmit power on the proposed RIS-aided cell-free network, we present the average weighted sum-rate against the BS transmit power in Fig. 7. It can be seen that, with the increase of the BS transmit power, the weighted sum-rate rises rapidly in all cases, which indicates the intuitive conclusion that increasing the transmit power can be a straightforward way to improve the WSR in the proposed network. However, we have a more important finding that, the performance gain brought by RISs is significant only when the BS transmit power is moderate (e.g., from -20 dB to 0 dB), while the performance gain becomes negligible when the BS transmit power is too low (e.g. -40 dB) or too high (e.g. 10 dB). The reason is that, the reflected signal by RIS is too weak when the BS transmit power is too low, while the received signal at the user is dominated by the direct BS-user link instead of the indirect BS-RIS-user link when the BS transmit power is too high due to the double-fading effect of the RIS. Particularly, with the increase of the BS transmit power, the link gain difference between the direct and indirect links becomes larger, thus the BSs tend to directly orient the beam towards the users, which makes the role of RISs less obvious. That is to say, when the BS transmit power is high enough, simply increasing it will weaken the benefits brought by RISs. Therefore, to improve the performance of the proposed RIS-aided cell-free network more cost and power effective, we should choose the appropriate BS transmit power<sup>3</sup>.

2) *Weighted sum-rate against number of BS/user antennas:* Then, we investigate the effect of the number of BS and user antennas. We plot the average weighted sum-rate against the number of BS antennas in Fig. 8, and that against the number of user antennas in Fig. 9, respectively. The general trend of the curves is consistent with the expectation, since we can see that the performance will be increased with the

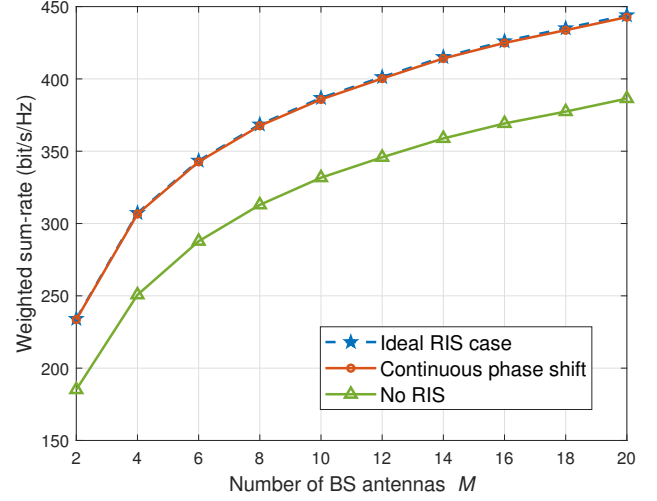


Fig. 8. Weighted sum-rate against the number of BS antennas.

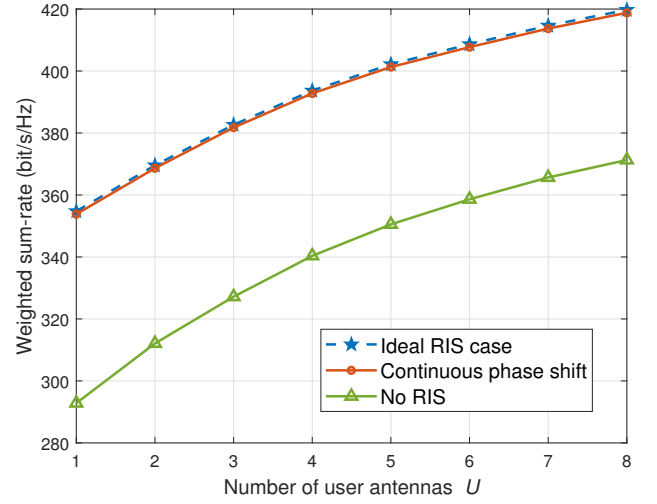


Fig. 9. Weighted sum-rate against the number of user antennas.

number of BS/user antennas. However, since the dimension of  $\mathbf{W}$  is  $BMPK$ , the complexity of solving (25) grows rapidly with the number of BS antennas number  $M$ , and the increase of user antennas also improve the complexity of matrix inversion in (15). Besides, too many antennas also makes the channel estimation more challenging. Therefore, in practical systems, we should choose the reasonable number of antennas to enhance the network capacity.

3) *Weighted sum-rate against number of RIS elements:* At last, the average weighted sum-rate against the number of RIS elements is shown in Fig. 10. We can see that the WSR performance gain of the RIS-aided cell-free network increases as the number of RIS elements rises, because more RIS elements provide higher beamforming gain. As the RIS is low-cost and energy-efficient, we can come to the conclusion that increasing the number of RIS elements can be a cost-effective way to improve the performance. More importantly, we can find an interesting observation that, with the increase

<sup>3</sup>In this paper, we only consider the transmit power, while the hardware power consumption and the corresponding energy efficiency optimization for the proposed RIS-aided cell-free network are left for future work.

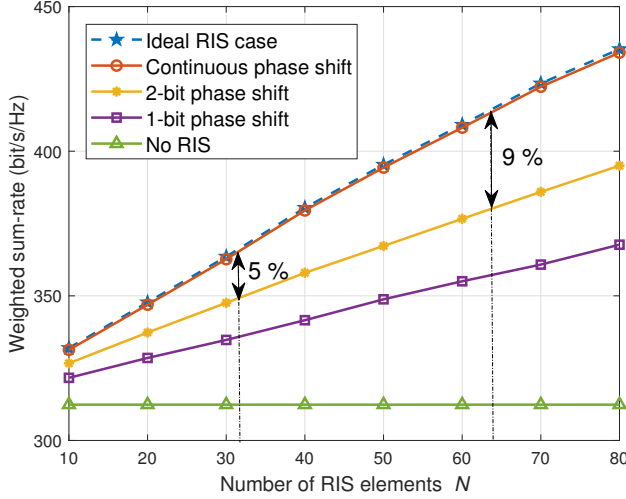


Fig. 10. Weighted sum-rate against the number of RIS elements.

of RIS elements, the approximation loss of the low-resolution phase shift becomes larger. For instance, when  $N = 32$ , the approximation loss in the case 2-bit phase shift is about 5% of the ideal case, and this loss grows to 9% when  $N = 64$ . The observation implies that, when the number of RIS is large, it is necessary to use more accurate phase shifts for passive precoding, so that the signals reflected from RISs can reach the users more precisely. In addition, since the dimension of  $\Theta$  is  $RN$ , the complexity of solving (37) grows with the number of RIS elements  $N$ , and too more RIS elements will also make the channel estimation and hardware implementation more challenging. Thus, it is essential to choose the number of RIS elements reasonably.

## V. CONCLUSIONS AND FUTURE WORKS

In this paper, we first propose the concept of RIS-aided cell-free network, which aims to improve the network capacity with low cost and power consumption. Then, for the proposed RIS-aided cell-free network, in the typical wideband scenario, we formulate the joint precoding design problem to maximize the weighted sum-rate of all users to optimize the network capacity, subject to the transmit power constraint of BS and the phase shift constraint of RIS. Finally, we propose a joint precoding framework to solve this problem. Since most of the considered scenarios in existing works are special cases of the general scenario in this paper, the proposed joint precoding framework can also serve as a general solution to maximize the capacity in most of existing RIS-aided scenarios. The simulation results demonstrate that, with the assist of low-cost and energy-efficient RISs, the proposed RIS-aided cell-free network can realize higher capacity than the conventional cell-free network.

For the proposed concept of RIS-aided cell-free network, only the weighted sum-rate maximization is considered in this paper, while some other important performance metrics such as the energy efficiency [15], BS transmit power [17], user SINR [22], [27], and secrecy rate [32] are left for future

works. Moreover, since the perfectly known CSI is assumed in this paper, the challenging problem of channel estimation [21] should be studied. In addition, the fully digital precoding at the BSs is considered in this paper, while the more energy-efficient hybrid precoding [40] can be investigated in future works.

## APPENDIX A PROOF OF LEMMA 1

From  $\mathbf{w}_{p,k} = [\mathbf{w}_{1,k,p}^T, \dots, \mathbf{w}_{B,k,p}^T]^T$ , firstly we can set  $b$  to 1 as an instance, and then obtain:

$$\mathbf{w}_{1,p,k} = \begin{bmatrix} \mathbf{I}_M & \cdots & \mathbf{0}_M \\ \vdots & \ddots & \vdots \\ \mathbf{0}_M & \cdots & \mathbf{0}_M \end{bmatrix} \mathbf{w}_{p,k} = \{(\mathbf{e}_1 \mathbf{e}_1^H) \otimes \mathbf{I}_M\} \mathbf{w}_{p,k}, \quad (46)$$

where  $\mathbf{e}_1 \in \mathbb{R}^B$  holds. This operation is essentially to take out the elements correlated with the first BS in  $\mathbf{w}_{p,k}$ . Since  $(\mathbf{e}_1 \mathbf{e}_1^H) \otimes \mathbf{I}_M$  is a diagonal matrix and all non-zero elements are 1, we have

$$\{(\mathbf{e}_1 \mathbf{e}_1^H) \otimes \mathbf{I}_M\}^H \{(\mathbf{e}_1 \mathbf{e}_1^H) \otimes \mathbf{I}_M\} = (\mathbf{e}_1 \mathbf{e}_1^H) \otimes \mathbf{I}_M. \quad (47)$$

Thus the power of  $\mathbf{w}_{1,p,k}$  can be represented as

$$\begin{aligned} \|\mathbf{w}_{1,p,k}\|^2 &= \mathbf{w}_{p,k}^H \{(\mathbf{e}_1 \mathbf{e}_1^H) \otimes \mathbf{I}_M\}^H \{(\mathbf{e}_1 \mathbf{e}_1^H) \otimes \mathbf{I}_M\} \mathbf{w}_{p,k} \\ &= \mathbf{w}_{p,k}^H \{(\mathbf{e}_1 \mathbf{e}_1^H) \otimes \mathbf{I}_M\} \mathbf{w}_{p,k}. \end{aligned} \quad (48)$$

Then, based on the definition  $\mathbf{W} = [\mathbf{w}_{1,1}^T, \mathbf{w}_{1,2}^T, \dots, \mathbf{w}_{1,K}^T, \mathbf{w}_{2,1}^T, \mathbf{w}_{2,2}^T, \dots, \mathbf{w}_{P,K}^T]^T$ , we obtain

$$\begin{aligned} &\sum_{k=1}^K \sum_{p=1}^P \|\mathbf{w}_{1,p,k}\|^2 \\ &= \sum_{k=1}^K \sum_{p=1}^P \mathbf{w}_{p,k}^H \{(\mathbf{e}_1 \mathbf{e}_1^H) \otimes \mathbf{I}_M\} \mathbf{w}_{p,k} \\ &= \mathbf{W}^H \begin{bmatrix} (\mathbf{e}_1 \mathbf{e}_1^H) \otimes \mathbf{I}_M & & \\ & \ddots & \\ & & (\mathbf{e}_1 \mathbf{e}_1^H) \otimes \mathbf{I}_M \end{bmatrix} \mathbf{W} \\ &= \mathbf{W}^H \{ \mathbf{I}_{PK} \otimes \{(\mathbf{e}_1 \mathbf{e}_1^H) \otimes \mathbf{I}_M\} \} \mathbf{W} \\ &= \mathbf{W}^H \mathbf{D}_1 \mathbf{W} \leq P_{1,\max}. \end{aligned} \quad (49)$$

Then, by setting  $b$  to other elements in  $\mathcal{B}$ , we can similarly deduce all expressions of the power constraints by

$$\mathbf{W}^H \mathbf{D}_b \mathbf{W} \leq P_{b,\max}, \quad \forall b \in \mathcal{B}, \quad (50)$$

where  $\mathbf{D}_b = \mathbf{I}_{PK} \otimes \{(\mathbf{e}_b \mathbf{e}_b^H) \otimes \mathbf{I}_M\}$ .

## APPENDIX B FEASIBLE SOLUTION TO PROBLEM (25)

We consider to solve (25) via Lagrange dual decomposition. By introducing  $\boldsymbol{\lambda} = [\lambda_1, \dots, \lambda_B]^T \in \mathbb{R}^B$ , we can equivalently transform (25) as

$$\begin{aligned} \min_{\boldsymbol{\lambda}} \quad & \Pi_1(\boldsymbol{\lambda}) = \max_{\mathbf{W}} \{ \Gamma_1(\mathbf{W}, \boldsymbol{\lambda}) \} \\ \text{s.t.} \quad & \lambda_b \geq 0, \quad \forall b \in \mathcal{B}, \end{aligned} \quad (51)$$

where

$$\Gamma_1(\mathbf{W}, \boldsymbol{\lambda}) = g_3(\mathbf{W}) - \sum_{b=1}^B \lambda_b (\mathbf{W}^H \mathbf{D}_b \mathbf{W} - P_{b,\max}). \quad (52)$$

Since the problem satisfies the Slater's condition, the duality gap does not exist strictly [48]. Then, by substituting  $g_3$  into (42) and setting  $\partial \Gamma_1 / \partial \mathbf{W}$  to zero, we obtain

$$\mathbf{W}^{\text{opt}} = \left( \sum_{b=1}^B \lambda_b \mathbf{D}_b + \mathbf{A} \right)^{-1} \mathbf{V}. \quad (53)$$

Finally, the optimal dual variable vector  $\boldsymbol{\lambda}^{\text{opt}}$  can be obtained via the ellipsoid method [48].

## APPENDIX C

### FEASIBLE SOLUTION TO PROBLEM (37)

Similarly, we consider to solve (37) via Lagrange dual decomposition. To simplify the expression, we use the following equivalent definition  $\mathcal{F}$  in (37) as

$$\mathcal{F} \triangleq \left\{ \theta_{r,n} \mid |\theta_{r,n}| \leq 1 \right\} \triangleq \left\{ \theta_{r,n} \mid |\theta_{r,n}|^2 \leq 1 \right\}. \quad (54)$$

Then, by introducing the dual variable vector  $\boldsymbol{\chi} = [\chi_{1,1}, \chi_{1,2}, \dots, \chi_{1,N}, \chi_{2,1}, \chi_{2,2}, \dots, \chi_{R,N}]^T \in \mathbb{R}^{RN}$ , the problem (37) can be equivalently transformed as

$$\begin{aligned} \min_{\boldsymbol{\chi}} \quad & \Pi_2(\boldsymbol{\chi}) = \max_{\boldsymbol{\Theta}} \{ \Gamma_2(\boldsymbol{\Theta}, \boldsymbol{\chi}) \} \\ \text{s.t.} \quad & \chi_{r,n} \geq 0, \forall r \in \mathcal{R}, \forall n \in \mathcal{N}, \end{aligned} \quad (55)$$

where

$$\begin{aligned} \Gamma_2(\boldsymbol{\Theta}, \boldsymbol{\chi}) &= g_7(\boldsymbol{\Theta}) - \sum_{r=1}^R \sum_{n=1}^N (|\theta_{r,n}|^2 - 1) \\ &= g_7(\boldsymbol{\Theta}) - \sum_{r=1}^R \sum_{n=1}^N (\chi_{r,n} \boldsymbol{\theta}^H \mathbf{e}_j \mathbf{e}_j^H \boldsymbol{\theta} - 1). \end{aligned} \quad (56)$$

Note that  $j = N(r-1) + n$  holds and  $\mathbf{e}_j \in \mathbb{R}^{RN}$ . Similarly, the problem also satisfies the Slater's condition and the duality gap doesn't exist [48]. Then, by setting  $\partial \Gamma_2 / \partial \boldsymbol{\Theta}$  to zero, we have

$$\boldsymbol{\theta}^{\text{opt}} = \left( \sum_{r=1}^R \sum_{n=1}^N \chi_{r,n} \mathbf{e}_j \mathbf{e}_j^H + \mathbf{\Lambda} \right)^{-1} \boldsymbol{\nu}. \quad (57)$$

Finally, the optimal dual variable vector  $\boldsymbol{\chi}^{\text{opt}}$  can be obtained via the ellipsoid method [48].

## REFERENCES

- [1] D. Lopez-Perez, M. Ding, H. Claussen, and A. H. Jafari, "Towards 1 Gbps/UE in cellular systems: Understanding ultra-dense small cell deployments," *IEEE Commun. Surveys Tuts.*, vol. 17, no. 4, pp. 2078–2101, Fourthquarter 2015.
- [2] F. E. Idachaba, "5G networks: Open network architecture and densification strategies for beyond 1000x network capacity increase," in *Proc. 2016 Future Technologies Conference (FTC'16)*, Dec. 2016, pp. 1265–1269.
- [3] W. Yu, H. Xu, H. Zhang, D. Griffith, and N. Golmie, "Ultra-dense networks: Survey of state of the art and future directions," in *Proc. 2016 25th International Conference on Computer Communication and Networks (ICCCN'16)*, Aug. 2016, pp. 1–10.
- [4] M. Kamel, W. Hamouda, and A. Youssef, "Ultra-dense networks: A survey," *IEEE Commun. Surveys Tuts.*, vol. 18, no. 4, pp. 2522–2545, Fourthquarter 2016.
- [5] J. G. Andrews, X. Zhang, G. D. Durgin, and A. K. Gupta, "Are we approaching the fundamental limits of wireless network densification?" *IEEE Commun. Mag.*, vol. 54, no. 10, pp. 1558–1896, Oct. 2016.
- [6] A. Lozano, R. W. Heath, and J. G. Andrews, "Fundamental limits of cooperation," *IEEE Trans. Inf. Theory*, vol. 59, no. 9, pp. 5213–5226, Sep. 2013.
- [7] E. Nayebi, A. Ashikhmin, T. L. Marzetta, and H. Yang, "Cell-free massive MIMO systems," in *Proc. 2015 49th Asilomar Conference on Signals, Systems and Computers (ACSSC'15)*, Nov. 2015, pp. 695–699.
- [8] G. Interdonato, E. Björnson, H. Q. Ngo, P. Frenger, and E. G. Larsson, "Ubiquitous cell-free massive MIMO communications," *arXiv preprint arXiv:1804.03421*, Apr. 2019.
- [9] H. Q. Ngo, A. Ashikhmin, H. Yang, E. G. Larsson, and T. L. Marzetta, "Cell-free massive MIMO versus small cells," *IEEE Trans. Wireless Commun.*, vol. 16, no. 3, pp. 1834–1850, Mar. 2017.
- [10] S. Mosleh, H. Almosa, E. Perrins, and L. Liu, "Downlink resource allocation in cell-free massive MIMO systems," in *Proc. 2019 International Conference on Computing, Networking and Communications (ICNC'19)*, Feb. 2019, pp. 883–887.
- [11] M. Attarifar, A. Abbasfar, and A. Lozano, "Modified conjugate beamforming for cell-free massive MIMO," *IEEE Commun. Lett.*, vol. 8, no. 2, pp. 616–619, Apr. 2019.
- [12] Y. Jin, J. Zhang, S. Jin, and B. Ai, "Channel estimation for cell-free mmwave massive MIMO through deep learning," *IEEE Trans. Veh. Technol.*, vol. 68, no. 10, pp. 10 325–10 329, Oct. 2019.
- [13] Y.-C. Liang, R. Long, Q. Zhang, J. Chen, H. V. Cheng, and H. Guo, "Large intelligent surface/antennas (LISA): Making reflective radios smart," *arXiv preprint arXiv:1906.06578*, Jun. 2019.
- [14] E. Basar, M. D. Renzo, J. de Rosny, M. Debbah, M.-S. Alouini, and R. Zhang, "Wireless communications through reconfigurable intelligent surfaces," *arXiv preprint arXiv:1906.09490*, Jun. 2019.
- [15] C. Huang, A. Zappone, G. C. Alexandropoulos, M. Debbah, and C. Yuen, "Reconfigurable intelligent surfaces for energy efficiency in wireless communication," *IEEE Trans. Wireless Commun.*, vol. 18, no. 8, pp. 4157–4170, Aug. 2019.
- [16] K. Ntontin, M. D. Renzo, J. Song, F. Lazarakis, J. de Rosny, D. T. Phan-Huy, O. Simeone, R. Zhang, M. Debbah, G. Leroosey, M. Fink, S. Tretjakov, and S. Shamai, "Reconfigurable intelligent surfaces vs. relaying: Differences, similarities, and performance comparison," *arXiv preprint arXiv:1908.08747*, Aug. 2019.
- [17] Q. Wu and R. Zhang, "Beamforming optimization for wireless network aided by intelligent reflecting surface with discrete phase shifts," *IEEE Trans. Commun. (early access article)*, 2019.
- [18] P. Wang, J. Fang, X. Yuan, Z. Chen, H. Duan, and H. Li, "Intelligent reflecting surface-assisted millimeter wave communications: Joint active and passive precoding design," *arXiv preprint arXiv:1908.10734*, Aug. 2019.
- [19] C. Pan, H. Ren, K. Wang, W. Xu, M. ElKashlan, A. Nallanathan, and L. Hanzo, "Multicell MIMO communications relying on intelligent reflecting surface," *arXiv preprint arXiv:1907.10864*, Jul. 2019.
- [20] C. Huang, C. Zhang, J. Yang, B. Sun, B. Zhao, and X. Luo, "Reconfigurable metasurface for multifunctional control of electromagnetic waves," *Adv. Opt. Mater.*, vol. 5, no. 22, p. 1700485, Sep. 2017.
- [21] C. Hu and L. Dai, "Two-timescale channel estimation for reconfigurable intelligent surface aided wireless communications," *arXiv preprint arXiv:1912.07990*, Dec. 2019.
- [22] Q.-U.-A. Nadeem, A. Kammoun, A. Chaaban, M. Debbah, and M.-S. Alouini, "Asymptotic analysis of large intelligent surface assisted MIMO communication," *arXiv preprint arXiv:1903.08127*, Mar. 2019.
- [23] L. Dai, B. Wang, M. Wang, X. Yang, J. Tan, S. Bi, S. Xu, F. Yang, Z. Chen, M. D. Renzo, and L. Hanzo, "Reconfigurable intelligent surface-based wireless communication: Antenna design, prototyping and experimental results," *arXiv preprint arXiv:1912.03620*, Dec. 2019.
- [24] Q. Wu and R. Zhang, "Intelligent reflecting surface enhanced wireless network: Joint active and passive beamforming design," in *Proc. 2018 IEEE Global Communications Conference (GLOBECOM'18)*, Dec. 2018, pp. 1–6.
- [25] C. Huang, A. Zappone, M. Debbah, and C. Yuen, "Achievable rate maximization by passive intelligent mirrors," in *Proc. 2018 IEEE International Conference on Acoustics, Speech and Signal Processing (ICASSP'18)*, Apr. 2018, pp. 3714–3718.
- [26] H. Li, R. Liu, M. Li, and Q. Liu, "IRS-enhanced wideband MU-MISO-OFDM communication systems," *arXiv preprint arXiv:1909.11314*, Sep. 2019.
- [27] H. Xie, J. Xu, and Y.-F. Liu, "Max-min fairness in IRS-aided multi-cell MISO systems via joint transmit and reflective beamforming," *arXiv preprint arXiv:1912.12827*, Dec. 2019.

- [28] J. Ye, S. Guo, and M.-S. Alouini, "Joint reflecting and precoding designs for SER minimization in reconfigurable intelligent surfaces assisted MIMO systems," *arXiv preprint arXiv:1906.11466*, Jun. 2019.
- [29] B. Di, H. Zhang, L. Song, Y. Li, Z. Han, and H. V. Poor, "Hybrid beamforming for reconfigurable intelligent surface based multi-user communications: Achievable rates with limited discrete phase shifts," *arXiv preprint arXiv:1910.14328*, Oct. 2019.
- [30] Y. Yang, S. Zhang, and R. Zhang, "IRS-enhanced OFDM: Power allocation and passive array optimization," *arXiv preprint arXiv:1905.00604*, May 2019.
- [31] X. Liu, Y. Liu, Y. Chen, and H. V. Poor, "RIS enhanced massive non-orthogonal multiple access networks: Deployment and passive beamforming design," *arXiv preprint arXiv:2001.1036*, Jan. 2020.
- [32] X. Yu, D. Xu, and R. Schober, "Enabling secure wireless communications via intelligent reflecting surfaces," *arXiv preprint arXiv:1904.09573*, Apr. 2019.
- [33] S. Li, B. Duo, X. Yuan, Y.-C. Liang, and M. D. Renzo, "Reconfigurable intelligent surface assisted UAV communication: Joint trajectory design and passive beamforming," *arXiv preprint arXiv:1908.04082*, Aug. 2019.
- [34] K. Shen and W. Yu, "Fractional programming for communication systems part I: Power control and beamforming," *IEEE Trans. Signal Process.*, vol. 66, no. 10, pp. 2616–2630, May 2018.
- [35] —, "Fractional programming for communication systems part II: Uplink scheduling via matching," *IEEE Trans. Signal Process.*, vol. 66, no. 10, pp. 2631–2644, May 2018.
- [36] U. Siddique, H. Tabassum, and E. Hossain, "Downlink spectrum allocation for in-band and out-band wireless backhauling of full-duplex small cells," *IEEE Trans. Commun.*, vol. 65, no. 8, pp. 3538–3554, Aug. 2017.
- [37] E. Nayebi, A. Ashikhmin, T. L. Marzetta, H. Yang, and B. D. Rao, "Precoding and power optimization in cell-free massive MIMO systems," *IEEE Trans. Wireless Commun.*, vol. 16, no. 7, pp. 4445–4459, Jul. 2017.
- [38] X. Hu, C. Zhong, X. Chen, W. Xu, and Z. Zhang, "Rate analysis and ADC bits allocation for cell-free massive MIMO systems with low resolution ADCs," in *Proc. 2018 IEEE Global Communications Conference (GLOBECOM'18)*, Dec. 2018, pp. 1–6.
- [39] S. Kusaladharma, W. P. Zhu, W. Ajib, and G. Amarasureya, "Achievable rate analysis of NOMA in cell-free massive MIMO: A stochastic geometry approach," in *Proc. 2019 IEEE International Conference on Communications (ICC'19)*, May 2019, pp. 1–6.
- [40] X. Gao, L. Dai, S. Han, C.-L. I, and R. W. Heath, "Energy-efficient hybrid analog and digital precoding for mmwave MIMO systems with large antenna arrays," *IEEE J. Sel. Areas Commun.*, vol. 34, no. 4, pp. 998–1009, Apr. 2016.
- [41] Q. Wu and R. Zhang, "Intelligent reflecting surface enhanced wireless network via joint active and passive beamforming," *IEEE Trans. Wireless Commun.*, vol. 18, no. 11, pp. 5394–5409, Nov. 2019.
- [42] M. Grant and S. Boyd, "CVX: Matlab software for disciplined convex programming, version 2.1," Mar. 2014.
- [43] H. Guo, Y.-C. Liang, J. Chen, and E. G. Larsson, "Weighted sum-rate optimization for intelligent reflecting surface enhanced wireless networks," *IEEE Trans. Wireless Commun. (early access article)*, 2020.
- [44] Q.-U.-A. Nadeem, A. Kammoun, A. Chaaban, M. Debbah, and M.-S. Alouini, "Asymptotic analysis of large intelligent surface assisted MIMO communication," *arXiv preprint arXiv:1903.08127*, Mar. 2019.
- [45] X. Gao, L. Dai, Y. Sun, S. Han, and C.-L. I, "Machine learning inspired energy-efficient hybrid precoding for mmwave massive MIMO systems," in *Proc. 2017 IEEE International Conference on Communications (ICC'17)*, May 2017, pp. 1–6.
- [46] . zdogan, E. Bjrnson, and E. G. Larsson, "Intelligent reflecting surfaces: Physics, propagation, and pathloss modeling," *IEEE Wireless Commun. Lett. (early access article)*, 2019.
- [47] J. D. Griffin and G. D. Durgin, "Complete link budgets for backscatter-radio and RFID systems," *IEEE Trans. Antennas Propag.*, vol. 51, no. 2, pp. 11–25, Apr. 2009.
- [48] S. Boyd and L. Vandenberghe, "Convex optimization," *Cambridge University Press*, 2004.